# Modeling for acoustic wave propagation in a thin plate with localized contact acoustic nonlinearity

Marina Terzi, Vladislav Aleshin, Lynda Chehami, Emmanuel Moulin

16ème Congrès Français d'Acoustique
11-15 Avril 2022, Marseille

# Modeling for acoustic wave propagation in a thin plate with localized contact acoustic nonlinearity

M. Terzi [a], V. Aleshin [b], L. Chehami [a], E. Moulin [a],
[a] Université Polytechnique des Hauts de France, IEMN-DOAE, Campus Mont Houy, 59313 Valenciennes, France
[b] Université de Lille, CNRS, Centrale Lille, IEMN-LCI, 59650 Villeneuve d'Ascq, France,

In NDT or SHM problems, contact acoustic nonlinearity occurs in solid materials in the presence of damage (cracks, delaminations, etc.) or degraded joints (welds, glue joints). Damage of this type represents inner contacts of rough surfaces exited in SHM experiments by complex-shaped acoustic signals. This paper is concerned with numerical modeling for ultrasonic waves' propagation in a thin plate in the presence of localized contact acoustic nonlinearity (CAN) whose position is to be detected in a SHM experiment reported elsewhere. Two types of CAN are considered: a sphere pressed against a thin plate (Hertz-Mindlin CAN) that models real damage in the experiments and a more realistic contact of rough surfaces (Rough-Surface CAN). These contacts have specific normal and tangential load-displacement relationships computed via the previously developed method of memory diagrams in which Coulomb friction is taken into account. In the considered example, the mechanical contact is activated by the Lamb wave propagating in a thin plate. Using these relationships together with equations of motion, the CAN response to the Lamb wave excitation is computed in terms of normal and tangential forces as functions of time in the virtually punctual contact area. This response becomes a secondary wave source that generates a weak perturbation wave to be recorded in SHM experiments for the purpose of detection of the damage location. The developed modeling tool successfully describes the above-mentioned phenomena and imitates wave-CAN interactions in simplified 2D plate-like geometry. This numerical tool can be used as a prototype for real numerical support software accompanying structural health monitoring experiments.

# 1 Introduction

This paper describes physical modeling for ultrasonic wave propagation in a thin plate in the presence of localized contact acoustic nonlinearity. Our modeling is to accompany real experiments in which the contact is excited by the Lamb wave in a thin plate that generates a specific response in terms of contact loads that, in turn, perturbs the propagation medium and induces secondary waves in there. In experiments, the recorded and subsequently processed signals provide an image on which contact location can be seen. Here we attempt to correctly imitate contact-wave interactions in a restrained geometry that constitutes a plate fragment with certain boundary conditions. In that way, the objective consists in establishing physical grounds and developing a prototype of a numerical tool capable of describing realistic signals and geometries corresponding to existing nondestructive testing (NDT) and structural health monitoring (SHM) technologies [1, 2, 3, 4] of damage visualization. It is expected that the future tool will provide digital support for these techniques and will help quantify damage via theory and experiment comparison.

Frictional contacts that arise due to the presence of damage have complex hysteretic response to acoustic excitation. In experiments reported elsewhere [5] real localized damage is substituted with a sphere-plate contact. Indeed, it has been shown [9] that contact between rough surfaces (cracks, delaminations) can be effectively replaced by a pair of geometrically smooth axisymmetric bodies. Relying on this assumption, we consider a model contact nonlinearity of the Hertz-Mindlin type [7]. The known solution for contact load-displacement relationship has been recently generalized for arbitrary loading histories [11]. This approach called the Method of Memory Diagrams (MMD) provides normal and tangential (frictional) contact forces as functions of contact displacements generated by the propagated wave. These forces, in turn, represent a source of secondary waves emitted from a point-like contact zone.

The major outcome of this paper is a developed modeling tool that takes into account the above-mentioned phenomena and imitates contact-wave interactions in simplified 2D plate-like geometry. Primary waves propagating in the absence of damage (step 1) cause mechanical response from the contact nonlinearity (step 2) that becomes a source of secondary waves generated in the plate (step 3) considered here as a perturbation.

This paper is organized as follows. Section 2 recalls theoretical force-displacement relationship for axisymmetric bodies (e.g. sphere and plate). In section 3 mechanical responses to acoustic excitation for Hertz-Mindlin contact acoustic nonlinearity is compared to a crack-like one (rough-surface contact). Section 4 is concerned with the secondary waves generated by the Hertz-Mindlin contact in a thin plate. In section 5 we present a numerical tool that incorporated the three above steps; the major findings are outlined in Conclusion.

# 2 Force-displacement relationship for axisymmetric bodies in contact: method of memory diagrams

The classical problem for the force $N$ and displacement $a$ arising from the normal compression of two balls is solved by H. Hertz [6] who obtained the following result:

$$\begin{cases} N(a) = \frac{4}{3} R^{*1/2} a^{3/2} \\ c = \sqrt{Ra} \end{cases} \tag{1}$$

where $c$ is the radius of contact area, $E^*$ is effective elastic modulus and $R^*$ is effective radius are given by

$$\begin{cases} \frac{1}{E^*} = \frac{1-\nu_1^2}{E_1} + \frac{1-\nu_2^2}{E_2} \\ \frac{1}{R^*} = \frac{1}{R_1} + \frac{1}{R_2} \end{cases} \tag{2}$$

where $E_{1,2}$ are Young's moduli and $\nu_{1,2}$ are Poisson's ratios for materials in contact.

In the considered case radius of half-space $R_2 = \infty$ and, consequently, $R^* = R_1 = R$, where $R$ is the sphere's radius.

If the normal force is kept constant, tangential force $T$ is

related to tangential displacement $b$ for spherical bodies by the Hertz-Mindlin solution [7]:

$$\begin{cases} T = \dfrac{4\mu E^*}{3R^*}(c^3 - s^3) \\ b = \dfrac{\mu\theta}{R^*}(c^2 - s^2) \end{cases} \tag{3}$$

where $\mu$ is a dry friction coefficient, $c$ is a radius of a contact zone, $s$ is a radius of stick zone.

For the contact of arbitrary axisymmetric bodies with negligible dissimilarities of materials (reduced elastic friction principle [8]):

$$\begin{cases} T = \mu(N(c) - N(c = s)) \\ b = \theta\mu(a(c) - a(c = s)) \end{cases} \tag{4}$$

where $\theta$ is a constant depending on materials of contacting half-spaces (sphere and plate, steel and aluminum) [9]. The tangential interaction is determined by the difference between the actual normal load-displacement relationship and the same relationship in which the contact radius is replaced by the slip zone radius (so that the corresponding load is virtually reduced).

Suppose now that the forces (or displacements) loading the contact are not constant over time, but vary in an arbitrary manner, with their vectors not leaving the same plane. This means that the contact interaction is described by the relationship between the forces $N(t)$, $T(t)$ and displacements $a(t)$, $b(t)$. This relationship can be calculated using the Method of Memory Diagrams (MMD) that represents a semi-analytical solution to the problem in which all the key relationships are given analytically, but contain the coefficients determined by the algorithm.

These analytical relationships for tangential force $T$ and displacement $b$ are as follows

$$\begin{cases} b = \theta\mu \displaystyle\int_0^a D(\alpha)\mathrm{d}\alpha \\ T = \mu \displaystyle\int_0^a D(\alpha)\frac{\mathrm{d}N}{\mathrm{d}a}|_{a=\alpha}\mathrm{d}\alpha \end{cases} \tag{5}$$

where $D(\alpha)$ is an internal system function (memory diagram) that encapsulates all memory information.

The algorithm is discussed in detail in [10] and [11]. It updates the shape of the memory diagram each time as input parameters change by infinitely small increments $\Delta a$ and $\Delta b$ for the displacement-driven system. Thus, if the arguments in the problem are displacements and the functions are forces, then based on the known values $\Delta a$ and $\Delta b$, the algorithm calculates current change in the memory diagram $D(\alpha)$, which satisfies the first equation in (3) written for increments. The updated memory diagram is then used for calculating the force responses $\Delta N$ and $\Delta T$. The algorithm requires the normal loading curve $N(a)$, in which the entire system geometry is encoded.

# 3 Modeling for contact acoustic nonlinearities excited by the Lamb waves

In this section, contact forces excited by the Lamb wave for two types of contact acoustic nonlinearities will be calculated: for the Hertz-Mindlin contact acoustic nonlinearity (HM-CAN) and for rough surface contact acoustic nonlinearity (RS-CAN). Here the HM-CAN corresponds to the physical model for damage used in the experiments reported in [5] that represents a contact between a sphere and a plate. The RS-CAN refers to a more realistic case where a defect is a crack or a loose joint with rough surfaces. Both CANs produce nonlinear force reactions to acoustic excitation. In what follows we focus on the interaction of CANs and the Lamb wave in more detail.

## 3.1 Hertz-Mindlin contact

The model defect—small steel ball pressed against an aluminum plate—is excited by the A0 Lamb mode. Then the coordinates of the ball's center of mass supposed to be zero when the bodies are unstrained are given as a superposition of wave displacements ($u_x$, $u_y$) and contact displacements ($a$,$b$):

$$\begin{cases} x = b + u_x = 0 \\ y = a + u_y \end{cases} \tag{6}$$

The former equation takes into account that horizontal motion is prohibited by a device positioning the ball as done in the experiments [5] while the latter one is to be combined with the equation of motion:

$$m\frac{\partial^2 y}{\partial t^2} = N_0 - N(a) \tag{7}$$

with $m$, the mass of the sphere. Here $N0$ denotes a precompression force that has two components, elastic prestress and gravity, and is positive for the $y$-axis directed downward, whereas the normal contact reaction force $N(a)$ is directed upward. The geometry of the problem is illustrated in Figure 1.

The equation of motion has to be supplemented by the calculation of the normal and tangential contact forces discussed in the previous section given by

$$\begin{cases} N(a) = \frac{4}{3}R^{*1/2}a^{3/2} \\ T(b) = T_{MMD}(b, a) \end{cases} \tag{8}$$

where $T_{MMD}$ is an automated analytical solution given by the Method of Memory Diagrams [10].

To combine a stationary A0 Lamb mode with zero wave displacement at $t = 0$, we multiply the known A0 wave displacement [12] by the ramp function.

$$u_{x,y}(t) = u_{x,y}^{Lamb}(1 - e^{-t/t_{ramp}}) \tag{9}$$

A formal requirement on the ramp duration $t_{ramp} \gg 1/f$, where $f$ denotes acoustic excitation frequency, guarantees that the distortion introduced by using this technique is

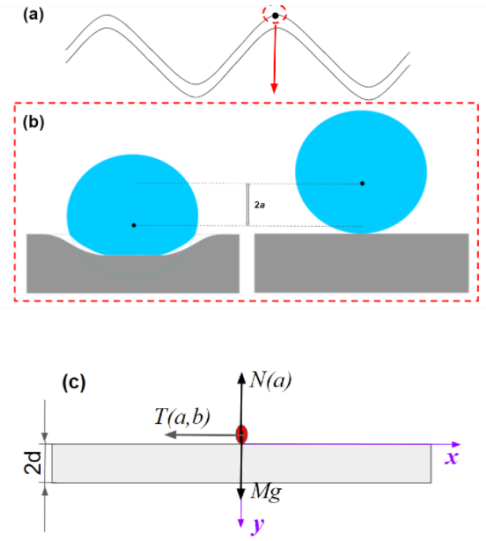


Figure 1: (a) Small ball pressed against a plate is excited by the Lamb wave (plate's deformation is highly exaggerated). (b) Zoom on the Hertz-Mindlin CAN. (c) Physical problem formulation for Hertz-Mindlin contact acoustic nonlinearity.

negligible. The initial condition $a = a_0$, with $a_0$, contact displacement produced by force $N0$, i.e. in the absence of the wave.

Due to the presence of the Hertz nonlinearity and of the hysteretic friction force, the equation of motion Eq. (7) together with Eq. (8) have to be solved numerically. Initial problems for ordinary differential equations are commonly solved by two numerical approaches: the Runge-Kutta and the Adams-Bashforth [13] methods. The both are precise and efficient enough and assume higher orders of approximation (e.g. 4th, 5th). However, the former one involves expressions to be calculated between time sampling points $t_j$, while the latter one is fully based on calculations at points $t_j$ only. Since the MMD does not directly provide any values between time sampling points, the Adams-Bashforth method is more appropriate in that case. Having this in mind, we rewrite the equations (7) and (8) to be solved in a form suitable for Adams-Bashforth method of the 5th order application:

$$\begin{cases} \dfrac{\mathrm{d}y}{\mathrm{d}t} = y_d \\ \dfrac{\mathrm{d}y_d}{\mathrm{d}t} = \frac{1}{m}(N0 - N|_{a=y-u_y(t)}) \end{cases} \tag{10}$$

in which the time derivative $y_d$ of the $y$-coordinate is defined explicitly. The numerical calculations are performed in accordance to the following scheme:

$$\begin{cases} y_{j+5} = y_{j+4} + \sum_{i=0}^{4} k_{i+1} f(t_{j=5-i}, y_{j=5-i}) \\ y_1 = a_0 \end{cases} \tag{11}$$

where $k_1 = \frac{1901}{720}$ , $k_2 = \frac{1387}{360}$, $k_3 = \frac{109}{30}$, $k_4 = \frac{637}{360}$, $k_5 = \frac{251}{720}$, $\mathrm{d}t$ is a time step with $f(t_i, y_i) = 0$ for $i$=1, 2, 3, 4. The latter equation indicates precompression at the initial moment of time.

Note that for making a new step in time the method requires knowledge of all variables on five previous time steps. This means that for five first steps of the algorithm, some of these previous values are not defined. However, since the procedure starts with zero initial conditions, we assume all such variables to be 0.

Calculation results for the HM-CAN exited by the Lamb wave obtained via the above method are considered later. Here we first concentrate on an analogous description for the RS-CAN.

## 3.2 Rough surface contact

The obvious difference between the case of real damage and the model Hertz-Mindlin CAN is that for real damage no additional mass has to be considered. The only inertial behavior for contact of rough surfaces can be associated with thin layers of material comprising surface roughness that can react on bulk load with some delay. However, the corresponding relaxation time is related to microstructure and is therefore much smaller than the acoustic period and thus is negligible. The quasi-static approximation for the boundary conditions at rough surfaces of real damage remains valid for any acoustic excitation of interest.

In the experiments and simulations for the Hertz-Mindlin CAN the ball is prestressed. A real crack can be prestressed either at least due to the following reason. During cracking, an external action is applied that separates crack faces by a distance significantly exceeding the atomic size. Upon releasing the action the crack faces tend to return back to the unstrained state, but due to micro-distortions of local surface shapes they can not do so with the atomic precision. The resulting shapes' mismatch acts as a thin layer of additional material "inserted" between crack faces which actually plays a role of prestress.

Implementing the above considerations, we assume the governing equation in the following form:

$$\begin{cases} a = a_0 - u_y \\ N = Ka^2 \\ x = b + u_x = 0 \\ T = T_{MMD}(b, a) \end{cases} \tag{12}$$

where $K = C^2 A_n$, $A_n$ is the nominal contact area and $C$ is a constant that can be either estimated from contact microgeometry parameters by using the model discussed in [11] or measured experimentally for a real contact in a way similar to Biwa et al. [14] $C = 6 \cdot 10^{10}$ Pa$^{1/2}$m$^{-1}$.

Here no mass is present so that the equation of motion is replaced by calculation of instantaneous reaction of the contact on the action of the Lamb wave. Displacement $a_0$ is responsible here for the prestress effect.

A graphical representation for the considered system is given in Fig. 2. The no-mass formulation corresponds to a contact between a surface and a small (much less than the wavelength) unmovable block whose coordinate $y$ always stays equal 0 and therefore is not introduced. Certainly, other configurations are possible, but the considered one

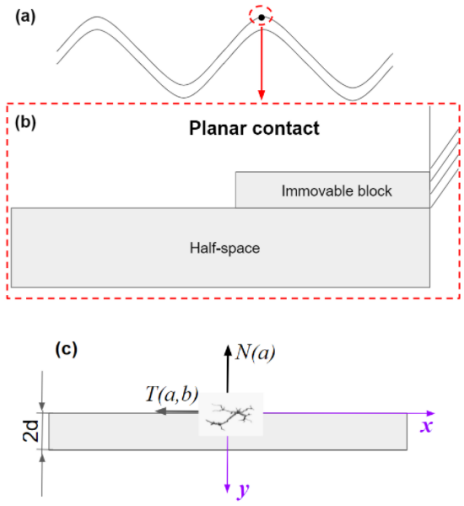


Figure 2: (a) A contact of rough surfaces is excited by the Lamb wave (plate's deformation is highly exaggerated). (b) Zoom on the RS-CAN. (c) Physical problem formulation for rough-surface contact acoustic nonlinearity.

fully corresponds to Eq. (12) and is geometrically similar to the Hertz-Mindlin CAN case.

### 3.3 Comparison of reactions of both CANs on acoustic excitation: results

Here it is appropriate to discuss the compliance between the model and real damage contact acoustic nonlinearities. Obviously, the powers in the normal reaction law are not the same in these cases (3/2 and 2). However, by selecting proper parameters, the normal load-displacement curves can be numerically matched. An example is shown in Figure 3 in which the Hertz-Mindlin and the rough-surface contact acoustic nonlinearities responses are qualitatively similar.

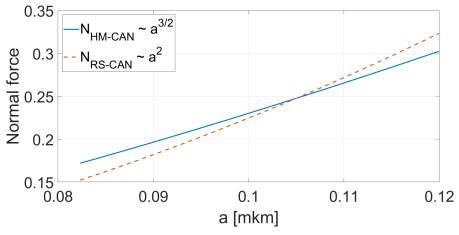


Figure 3: The normal load-displacement curve for the HM-CAN and a close curve for RS-CAN with matched parameters for $m^*$=414.

The rough-surface curve (RS-CAN) is matched to Hertz-Mindlin curve (HM-CAN) with the least squares method. Accepting the value of $C = 6 \cdot 10^{10}$ Pa$^{1/2}$m$^{-1}$ measured by Biwa et al. [14] for two aluminum blocks as a reference, we get the radius of nominal contact area $A_n \sim 6.24 \cdot 10^{-9}$ m$^2$ that corresponds to the contact size of $c \sim 4 \cdot 10^{-5}$m. This means that in both cases the contact size is much less than all macroscopic geometry dimensions (1 cm sphere, 1 m by 0.5 m by 3 mm plate) and thus can be considered as punctual.

Despite similar normal responses, the reaction of the considered CANs to the acoustic excitation can be different. The reason is in dynamic effects that arise in the HM-CAN with the finite mass but do not occur in the case of massless RS-CAN. In Figures 4 and 5, we illustrate cases of various strengths of the dynamic effects that consist in low-frequency modulation of the force and displacement responses and in a general loss of periodicity with $1/f$ period. In Figure 4 they are almost negligible while in Figure 5 their magnitude is significant.

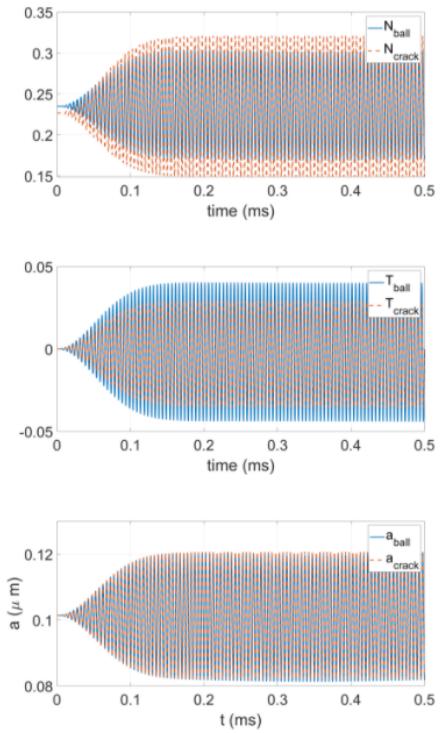


Figure 4: Normal (a) and tangential (b) forces applied to the plate by the HM-CAN and RS-CAN with matched normal responses $N(a)$. Here $m^*$=414 indicating weak dynamic effects. (c) Normal displacement produced by the HM-CAN and RS-CAN with matched normal responses $N(a)$.

It is easy to quantify the expected dynamic effect level by calculating of the dimensionless mass $m^*$ appearing in the dimensionless form of Eqs.(6)-(9) for the HM-CAN:

$$m^* = \frac{a_0 m f^2}{N0} \tag{13}$$

is a combination of the inverse normal stiffness $a_0$/N0 and the known parameter $mf^2$. To reduce the dynamic effects and make the HM model more adequate to real damage with no inertia, one has to increase the dimensionless mass $m^*$ by increasing the real mass, exciting the plate with a higher frequency, or having a less stiff contact. In Figures 4 and 5 the parameter $m^*$ equals 414 and 155, respectively.

It is also important to mention that increasing prestress reduces the nonlinearity of the problem. Nevertheless, the

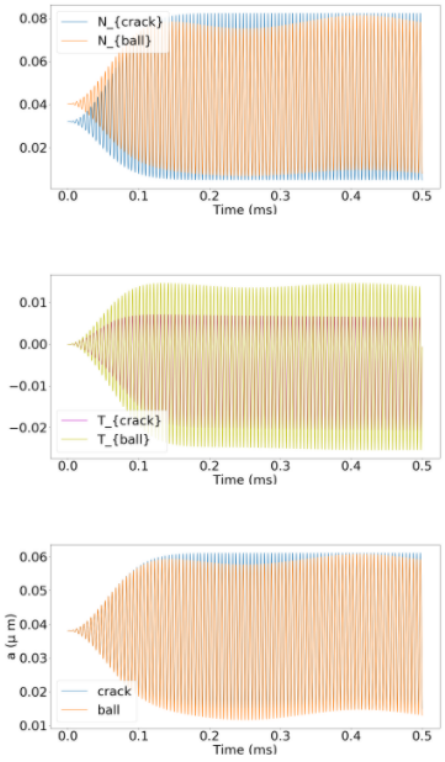


Figure 5: Normal (a) and tangential (b) forces applied to the plate by the HM-CAN and RS-CAN with matched normal responses $N(a)$. Here $m^*$=155 that corresponds to moderate dynamic effects. This HM-CAN mimics real damage only qualitatively. (c) Normal displacement produced by the HM-CAN and RS-CAN with matched normal responses $N(a)$.

secondary waves are generated even for high prestress levels making it possible to detect localized CAN position via methods developed in [5].

# 4 Secondary waves generated by contact acoustic nonlinearity in a thin plate

The obtained forces as functions of time can be interpreted as a secondary waves' source located at a small area (practically a point) on the plate surface. This section is concerned with the propagation problem for secondary waves excited by the CAN that plays a role of a punctual force source. The geometry of the problem is illustrated in Figure 6.

The plate top and bottom surfaces are considered free (zero normal stress). The conditions at the plate edges for the secondary wave problem represent zero displacements (fixed boundaries) to avoid activating the movement of the plate as a whole. Such movement would occur in a situation when the plate is excited by stresses or velocities without fixing displacements at least at some point of the boundary.

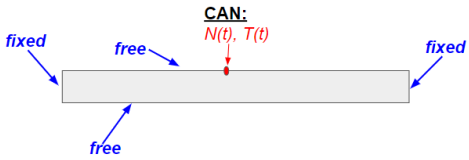


Figure 6: Geometry of the secondary wave generation problem. The CAN is excited by the A0 Lamb wave displacements and now, in turn, generates secondary waves via application of nonlinear punctual forces $N(t)$ and $T(t)$ calculated as explained in section 2.

In the experiment we simulate [5], the plate is suspended with elastic strings which are not considered in the present numerical model.

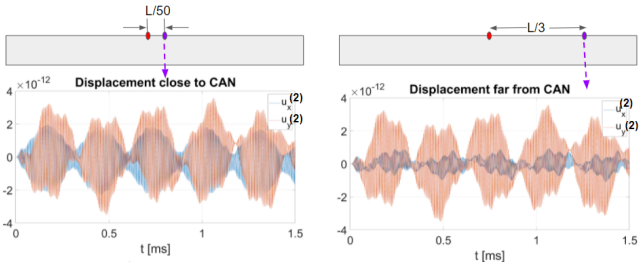


Figure 7: Secondary waves emitted by Hertz-Mindlin CAN in a thin plate.

A typical profile of the secondary wave excited by forces depicted in Figure 4 is shown in Figure 7. To see more features in the secondary wave, we have considered a long sequence of the force oscillations comprising 300 periods of the A0 Lamb wave (cf. 100 periods in Figure 4 for the forces). A quasi-periodic force protocol excites a long series of reverberations from the edges of the small plate fragment (Figure 7). The multiply reflected wave interferes with itself producing a complex non-periodic signal. The amplitude of the secondary waves is four orders of magnitude smaller than the amplitude of the primary waves. This proves that the considered contact acoustic nonlinearity is weak and justifies the use of the perturbation method in this modeling tool.

# 5 Prototype of numerical tool accompanying SHM experiments for detecting damage in thin plates

There exists a substantial difference in geometric parameters between the simplified case described via the developed modeling tool and real SHM experiments in thin plates. Due to this reason, the developed tool can be seen as a prototype for a future more advanced numerical toolbox capable of imitating realistic secondary waves emitted by damage that contain information for damage locating algorithms. However, the principal stages of the

modeling procedure are similar for both the prototype and a prospective working toolbox. The prototype tool comprises the following three steps.

1. Generation of stationary A0 Lamb wave or of a transitional wave process at a certain frequency in a fragment of a thin plate in the absence of a defect.
2. The equation of motion in ordinary derivatives for a Hertz-Mindlin CAN excited by wave displacements is numerically solved using the Adams-Bashforth algorithm in the purpose of obtaining the normal $N(t)$ and tangential $T(t)$ contact forces applied to the plate at the defect position. In the case of rough-surface CAN, these forces are calculated directly from the known contact displacements $a(t)$ and $b(t)$ without solving the equation of motion. In both situations, the load-displacement relationships for frictional contact are obtained with the use of the Method of Memory Diagrams. The corresponding algorithms are implemented in Fortran.
3. Solving the problem for secondary waves emitted by a punctual force with the normal $N(t)$ and tangential $T(t)$ components applied at the defect position (programmed in COMSOL Multiphysics). Same geometry as at step 1 is considered.

# 6 Conclusion

We developed a prototype of a support numerical tool for SHM experiments modeling acoustic wave propagation in a thin plate in the presence of contact acoustic nonlinearity (CAN). The comparison between the model CAN (sphere-plate contact or Hertz-Mindlin CAN) and crack-like damage (Rough Surface CAN) showed that there exist physical conditions under which their mechanical responses to acoustic excitation are qualitatively similar. Namely, the dimensionless mass introduced in Eq. (13) must be much higher than 1. Higher dimensionless mass provides the similarity between the both responses at a longer time interval. The developed numerical tool adequately describes the physical nature of the CAN-wave interaction, but the considered test geometry significantly differs from the experimental one. In the future, mutual compromises from both modeling and experimental sides can help reach a configuration which, on the one hand, assumes the application of the damage locating algorithms and visualizing damage, and, on the other hand, adequate modeling is possible. This effort would result in establishing a detailed theory and experiment agreement in NDT/SHM problems.

# Acknowledgements

The authors would like to thank the French National Agency (ANR) for financing this work as a part of the project "Passive Ambient Noise-based Structural monitoring through exploitation of Contact Acoustic Nonlinearity" (PANSCAN).

# References

[1] K. E. Thomenius, Evolution of ultrasound beamformers, *1996 IEEE Ultrasonics Symposium. Proceedings*, **2**, 1615–1622, San Antonio, TX, USA, (1996).

[2] J. C. P. McKeon and M. K. Hinders, Parallel projection and crosshole Lamb wave contact scanning tomography, *Journal of Acoustical Society of America*, **106**(5), 2568–2577 (1999).

[3] P. D. Wilcox, Omni-directional guided wave transducer arrays for the rapid inspection of large areas of plate structures, *IEEE Transactions on Ultrasonics, Ferroelectrics and Frequency Control*, **50**(6), 699–709 (2003).

[4] L. Chehami, E. Moulin, J. de Rosny, C. Prada, O. Bou Matar, F. Benmeddour, and J. Assaad. Detection and localization of a defect in a reverberant plate using acoustic field correlation, *Journal of Applied Physics*, **115**(10), 104901 (2014).

[5] M. Terzi, L. Chehami, M. Farin, E. Moulin, V. Aleshin, N. Smagin, J. de Rosny, and F. Benmeddour, Pump-probe localization technique of varying solid contacts, *Journal of Acoustical Society of America* **149**, 2943-2949 (2021).

[6] H. R. Hertz, Über die Berührung fester elastischer Körper und Über die Härte, *Verhandlungen des Vereins zur Beförderung des Gewerbefleisscs*, Berlin: Verein zur Beförderung des Gewerbefleisses, 449-463 (1882).

[7] R. D. Mindlin and H. Deresiewicz, Elastic Spheres in Contact Under Varying Oblique Forces, *Journal of Applied Mechanics*, **20**(3), 327–344, (1953).

[8] J. Jäger, A New Principle in Contact Mechanics, *Journal of Tribology*, **120**(4), 677–684, (1998).

[9] V. L. Popov and M. Heß, *Method of Dimensionality Reduction in Contact Mechanics and Friction*, Springer, Berlin [Heidelberg] (2015).

[10] V. Aleshin, O. Bou Matar, and K. Van Den Abeele, Method of memory diagrams for mechanical frictional contacts subject to arbitrary 2D loading, *International Journal of Solids and Structures*, 60-61: 84–95 (2015).

[11] V. V. Aleshin, S. Delrue, K. Van Den Abeele, and O. Bou Matar, Nonlinear and hysteretic constitutive models for wave propagation in solid media with cracks and contacts, in T. Kundu, *Nonlinear Ultrasonic and Vibro-Acoustical Techniques for Nondestructive Evaluation* (Chapter 5), 175–224, Springer, Cham, (2019).

[12] I. A. Viktorov, *Rayleigh and Lamb waves: physical theory and applications*, Springer Science + Business Media, New York (2013).

[13] E. Hairer, S. P. Nørsett, and G. Wanner, *Solving ordinary differential equations I: nonstiff problems*, Springer, Heidelberg, London, 2nd rev. edition (2009).

[14] S. Biwa, S. Nakajima, and N. Ohno, On the Acoustic Nonlinearity of Solid-Solid Contact With Pressure-Dependent Interface Stiffness, *Journal of Applied Mechanics*, **71**(4), 508–515 (2004).